Raman Spectroscopy of Carbon Materials

J.R. Dennison[*]
Physics Department, Utah State University, Logan UT 84322-4415

Mark Holtz
Physics Department, Texas Tech University, Lubbock TX 79409

Greg Swain
Chemistry and Biochemistry Department, Utah State University, Logan UT 84322-0300

[*]*Author to whom correspondence should be addressed.*

Use of carbon materials is no longer limited to diamond jewelry or graphite pencils and lubricants. The last decade has witnessed an explosion of technological applications driven by the development of fabrication methods and the discovery of several new classes of pure carbon. Structural diversity exhibited by the carbon atoms, from local chemical order to long-range crystalline order, is key to understanding their physical and chemical properties and in future materials development. This article summarizes the use of *Raman spectroscopy* as a principal tool to investigate the vibrational dynamics of carbon materials and to provide indirect structural characterization of their short-, medium- and long-range order.

Carbon exhibits unique versatility of its bonding chemistry among the elements. The existence of carbon two-fold (sp^1), three-fold (sp^2), and four-fold (sp^3) hybridized bonding types is responsible for the huge variety of more than ten million organic compounds. The multiplicity of carbon bonding configurations is also manifested in the remarkable diversity of stable phases of pure solid carbon (see Figure 1) (1-3). We can classify these solid carbon phases as *crystalline* [diamond, graphite, and fullerites], *disordered* [glassy carbon, nanocrystalline carbon, graphitic amorphous carbon (g-C), diamond-like amorphous carbon (d-C), tetrahedral amorphous carbon (a-tC), andeither diamond-like or polymer-like hydrogenated amorphous carbon (a-C:H) depending on H content], or *molecular* [fullerenes, graphenes and related materials].

The two most common crystalline forms of carbon, graphite and diamond, exhibit dramatic differences as a result primarily of short-range order (local or chemical order). The local bonding manifests itself in differences in electrical, optical, thermal, and mechanical properties of the two crystals. Diamond, which is formed with very strong and nearly isotropic tetrahedral sp^3 bonding, is hard and transparent, is an unsurpassed thermal conductor, and is an insulator with a large energy gap (4). Graphite, on the other hand, is a soft, black, layered semi-metal with extremely strong trigonal sp^2 planar bonding and weak interlayer π-bonds (1).

Amorphous carbon (a-C) also shows dramatic variations in macroscopic properties depending on the local structure and relative amounts of sp^2 and sp^3 bonding; this structure is dictated by the formation method, deposition substrate conditions, presence of hydrogen, and post-growth annealing (5-8). a-C ranges from soot-like g-C to optically transparent and extremely hard d-C films. Bandgaps range from $\bullet$0.5 eV for g-C to >4 eV for some d-C and a-C:H films (4,5). This diversity illustrates and emphasizes the importance of short-range and even medium-range order on the physical properties of carbon solids and the close ties between the bonding, structure, and other physical properties (9-10).

Recently, entirely new classes of stable solid-carbon structures have been identified (11,12). Fullerenes are pure carbon materials with trigonal bonding which form closed-form molecular structures composed of twelve pentagonal rings and additional hexagonal rings (13). These include the soccer ball-shaped C_{60}, the rugby ball-shaped C_{70}, and other sized molecules. Fullerites are crystalline solids with molecular fullerenes occupying each lattice site. Many

complex related structures are referred to as graphenes; two examples are nested fullerenes and carbon nanotubules (14,15).

The purpose of this review is to provide a basic template for identifying and understanding the Raman signatures of various carbon materials and for monitoring structural changes. We first outline experimental probes of carbon structure and recent advances in Raman instrumentation. This is followed by a description of Raman spectroscopy applied to the most commonly observed forms of solid carbon, as summarized in Table 1.

EXPERIMENTAL TECHNIQUES

The principal experimental probes of the structure of crystalline forms of carbon have been x-ray, neutron and electron diffraction. However, for disordered and molecular forms of carbon, diffraction is often insufficient to fully characterize the structure. Vibrational dynamics are intimately related to structure and have been used extensively as an indirect probe of the atomic order of carbonaceous materials (16). In particular, Raman spectroscopy has been proven to be extremely sensitive to short-, medium-, and long-range order in solid carbon and has become a standard technique in characterizing carbon materials. Nuclear magnetic resonance (NMR) spectroscopy has also been used to provide information about bonding (including the fraction of sp^2/sp^3 bonding) and short-range order in carbon materials (17). Infrared spectroscopy, inelastic neutron scattering, electron energy loss spectroscopy, EXAFS, and photoemission spectroscopy provide additional dynamical and indirect structural information (5,9).

Spontaneous Raman scattering is an inelastic light scattering process [refer to Figure 2(a)]. A simple picture of Raman scattering involves two processes: (A) incident light, usually from a laser, is absorbed by a polarizable sample, inducing a transition from the ground electronic state to an excited or “virtual” state, and (B) the energetic system then radiatively relaxes via a transition from the “virtual” state to a lower energy electronic state by spontaneous emission of a photon and either creating (Stokes process) or absorbing (anti-Stokes process) a vibrational quantum of energy (a phonon in crystals). The emitted photon is shifted in energy from the incident excitation photon energy, $h\nu_L$ by the phonon energy. Typically, only Stokes processes are studied, due to their higher intensities. Spectra of the intensity versus emission photon energy exhibit peaks at

energies $h\nu_S$ which correspond to the vibrational energies involved in the process. Vibrational energies are usually expressed in inverse wavelength ($1/\lambda=\Delta E/hc$, $\Delta E=h\nu_L-h\nu_S$) with units of cm^{-1} as is customary in infrared spectroscopy. In crystals, Raman selection rules dictate that only zone-center (those which retain the full symmetry of the crystal) optic (those having non-zero energy at the zone center) vibrations are allowed to participate in first-order Raman scattering (18).

Advances in Raman Instrumentation. The primary components of a Raman system include a continuous laser source (typically Ar or Kr ion lasers) focused onto the sample, a spectrometer for collecting and separating the scattered light into its component wavelengths, a detector, and controlling electronics (19). Traditionally, Raman measurements have been made using systems such as the one shown in Figure 2(b). Illumination is usually carried out with a 180E backscattering geometry which is suitable for thin films or when one has no *a priori* knowledge of the optical properties of the specimen (i.e., opaque or transparent samples). Polarization rotators, analyzers and scramblers are useful when polarization selection rules are important to understand. This can be especially relevant when measuring mixed phases, *e.g.* microcrystalline diamond and disordered phases (20). A collection objective guides the desired scattered light into the double-stage spectrometer which disperses the spectrum. The relative intensities of the undesired stray light and desired Raman scattering demand superior stray-laser-light rejection capabilities. A cooled photomultiplier is used in a photon counting mode to detect the light. Multichannel detection (21) significantly diminishes data collection times. These are used with double monochromators (with limited spectral range) or triple monochromators which are specifically suited to multichannel detection. Computer automation controls the spectrometer and stores the signal from the detector electronics for analysis.

The advent of narrow rejection range, holographic edge and notch filters (22) has made the use of a single-stage grating monochromator for Raman scattering possible [Figure 2(c)]. The importance of this innovation is two-fold. First, single-stage monochromators are optically fast. When coupled with a multichannel array, this allows for studies with low excitation intensities from delicate samples, makes plausible the study of weakly scattering materials, and permits rapid turn-around for process diagnosis. Second, suitable, high-quality, single-grating monochromators cost considerably less than traditional double monochromators commonly used in Raman

spectroscopy, although a small sacrifice in spectral resolution may result. We have found this type of system to be more than adequate for carbon solids (see, *e.g.*, Figure 3).

RAMAN CHARACTERIZATION OF SOLID CARBON

Diamond. Diamond has long been renowned for its superlative properties. It is the hardest natural substance, has the highest thermal conductivity, and is best known for its spectacular optical properties (1,4). The recent advent of methods, primarily through chemical vapor deposition (CVD), to readily produce synthetic bulk diamond and diamond films opens possibilities for many new applications (4,7,23). These include application as large band-gap, high temperature semiconductors, cold cathode emitters, protective optical or wear-resistant coatings, abrasive and cutting agents, optical materials, electrodes, and thermal dissipators.

The face-centered cubic (fcc) crystal structure of diamond, with complete tetrahedral bonding, is shown in Figure 1(a). Theoretical models are available for the vibrational dispersion, density of states and Raman spectrum of diamond (24).

The first order Raman spectrum of diamond [Figure 3(a)] has a single line at 1333"1 cm^{-1} identified as the three-fold degenerate, zone-center O(Γ) mode (25). This peak has an extremely narrow natural line width, on the order of 2 cm^{-1}. It broadens, but does not shift appreciably, for smaller crystallites found in natural diamonds, synthetic diamonds, and diamond films (20). An increase in intensity of the O(Γ) peak with increasing excitation energy has been attributed to resonance effects (26). Diamond films often exhibit weak, broad peaks near the main graphite 1581 cm^{-1} peak, which are interpreted as an indication of the presence of limited sp^2 bonding in the films (26).

Study of the effects of stress on the Raman spectrum of diamond offers valuable insight relavent to the mechanical and electronic applications of epitaxial diamond films as coatings and semiconductors. The O(Γ) peak shifts to higher wavenumbers with increased isotropic pressure and is almost linear up to at least 40 GPa (27). There is very little broadening with increased isotropic pressure, although uniaxial strain can reduce the cubic symmetry of diamond, thereby splitting the O(Γ) degeneracy and causing peak broadening (28,29). Compressive uniaxial stress X increases the Raman shifts for stresses along the <100> or <111> axes according to

$$X_{2<100>}\ (dyn/cm^2) = -1.08x10^{10}\ \Delta v_s\ (cm^{-1})$$

$$X_{2<111>}\ (dyn/cm^2) = -2.63x10^{10}\ \Delta v_s\ (cm^{-1})$$

where Δv_s is the shift of the observed singlet state from 1333 cm^{-1} (30). The strain (as a percent of the 3.567 Å unstrained bond length) can then be approximated using e (%) = 8.53⇳10^{-14} X (dyn/cm^2) (29).

Broadening is also observed due to substrate-induced uniaxial strain of epitaxial diamond films (30). Micro-Raman studies of CVD diamond films have revealed that shifting due to *local* strain may be responsible for the broadening observed in CVD diamond films (20). [Recent development of near-field scanning optical microscopy (NSOM) has pushed the range of micro-Raman below the Rayleigh resolution limit (30). This permits spatial resolution in the 20 to 50 nm range. However, due to low intensity throughput of the optical fiber used in NSOM, spectroscopic resolution is sacrificed resulting in large linewidths. Further work is necessary to boost signal/noise so that quantitative analysis can be achived.] We note briefly that if the lattice mismatch or growth conditions are not conducive to epitaxial growth, then polycrystalline film morphology may dominate. Under these conditions, studies cross-correlated with transmission electron micrographs are useful to obtain a full picture of the thin-film morphology. The frequency dependence of the O(Γ) peak due to isotopic content in diamond has Isotopic substitution has been successfully been measured and agrees with theory (32). used to study the function of gas-phase precursors in CVD grown diamond films (33). Johnson and Weimer examined the isotopic shifting of the disorder-related band (near 1500 cm^{-1} in their pure ^{12}C sample) when the ^{13}C content of acetylene and methane feed gases are varied. Excellent correlation is found with the ^{13}C content of the methane, but not with the acetylene, indicating that it is the methane which is responsible for disordered carbon in this case.

Spectral features in second order Raman spectra range between 2600 to 2900 cm^{-1} (25). The two-phonon overtone spectrum is proportional to the one-phonon vibrational density of states (VDOS) and has been used to accurately establish phonon energies and symmetries for many

phonon branches at all high-symmetry points in the Brillouin zone (25).

Graphite. Graphite has widespread applications due to its unique combination of physical properties. Weak interplanar bonding allow adjacent carbon planes to easily slide over one another, leading to use as a lubricant and for pencils. In contrast, the strong intraplanar covalent bonds lead to a high melting point with applications as a refractory-like material. The combination of high temperature stability, good electrical and thermal conductivity, and chemical inertness result in use as electrodes for spectrochemical analysis, electrochemistry, materials processing and electrical motors.

The hexagonal crystal structure of graphite is shown in Figure 1(b). Because the separation between planes is almost 2½ times the in-plane nearest-neighbor distance, graphite is often treated as being composed of 2D hexagonal sheets.

The theory and experimental measurements of the graphite vibration dispersion, density of states, and Raman spectrum are also well understood.(34,35) The first order Raman spectrum of crystalline graphite [see Figs. 3(c) and 4(a)] exhibits a very strong, high frequency, in-plane stretching mode (E_{2g}^2 or "G" peak) at 1581"1 cm^{-1} and a weaker low-frequency mode (E_{2g}^1) at 42"2 cm^{-1}.(36) The low-energy mode [see Figure 4(b)] corresponds to a phonon of the shear mode between adjacent planes. Graphite peaks have been observed to shift due to applied pressure and strain (37). Continuum scattering from 2200 cm^{-1} to 3250 cm^{-1} is observed in the second order Raman spectrum of graphite, with a strong feature near 2710 cm^{-1} and weaker features at 2450 cm^{-1} and 3250 cm^{-1} (38); these have been used to model the VDOS and finite size effects.(36,39) Resonance Raman behavior is observed in graphite; the most pronounced behavior for the 1581 cm^{-1} peak is attributed to π-π^* transitions. (39)

A diverse class of carbonaceous materials exhibits graphite (hexagonal) order at medium-range. Robertson (5) has identified a hierarchy of order range in graphitic carbon structure, beginning with single crystal graphite. The degree of order is characterized by the in-plane coherence length L_a of hexagonal order and the range of planar stacking L_c. Polycrystalline graphite exhibits varying degrees of crystalline order from highly oriented pyrolytic graphite [HOPG; L_a . 1 μm and L_c . 4 μm (2)] to "glassy", turbostratic, or nanocrystalline graphite and graphite fibers (L_a>1.5 nm and L_c . 1 nm).(3,5,40) Graphite is the most stable

equilibrium phase of carbon at low temperatures and pressures; most forms of carbon (except bulk diamond) exhibit thermally assisted transformation to graphite at modest temperatures. Pyrolysis of organic materials evolves volatile species (*e.g.*, H, N, O) during *carbonization*, typically in a range of temperatures from 400 EC to 700 EC. Formation of graphitic sheets of pyrolytic carbon (*polymerization*) typically occurs between 600 EC and 1200 EC. Annealing of such pyrolytic carbon at 1200˜T˜3000 EC produces gradual layering or ordering of the sheets (*graphitization*), eventually reaching a 3D lattice of crystalline graphite.(2,5)

Raman spectroscopy has been developed as a standard method for determining the planar coherence lengths (L_a) in graphitic carbon which possesses limited long-range order [Figure 3(d)].(41-44) For these materials, an additional broad band is found at . 1360 cm^{-1} (historically denoted with the misnomer "D" which can be considered a mnemonic for “Disordered”), which is attributed to disorder induced Raman activity of zone-boundary A_{1g} phonons.(44,45) For finite sized regions with graphite-like structure, a breakdown occurs in the Raman selection rules applicable to infinite crystals.(42,46) Tuinstra and Koenig used x-ray diffraction in parallel with Raman studies to show that the intensity ratio of the 1360 cm^{-1} peak to the E^2_{2g} peak is inversely proportional to L_a over a range of 2.5 nm to 1000 nm.(41,43,44) This has become an accepted technique for determining L_a in disordered graphitic materials. The disorder activated “D” band also exhibits a pronounced shift with laser photon energy. This shift is strong, ~50 cm^{-1}/eV, and as yet is not fully explained. The general aspects of this phenomenon have been summarized by McCreery and coauthors (47).

Recent work has extended the capabilities of Raman spectroscopy to investigate *both* the intraplanar and interplanar structure of graphitic carbon materials. Dallas *et al.* simultaneously determined the *intraplanar* coherence length L_a and the *interplanar* structure of nanocrystalline graphite, using a quantitative model which relates the average layer thickness (L_c) to an E^1_{2g} peak line shape analysis based on the dispersion of the phonons corresponding to interplanar shear motion [see Figure 4].(48) The E^1_{2g} mode is extremely sensitive to interplanar disorder, and should be absent if no planar structure exists. They found that laser ablation altered, but did not entirely destroy the layered structure of HOPG. The most disordered graphite studied had L_a . 6.0 nm (equivalent to a coherent region of ~600 graphite hexagonal rings) and L_c . 0.85 nm (an

average of ~2½ graphite planar spacings).

An additional weak feature at . 1620 cm^{-1} is sometimes observed in disordered graphite [see Figure 2(d)], which has been attributed to splitting of the degenerate E^2_{2g} peak (38) and to breakdown of the Raman selection rules allowing contribution from non-zone-center phonons.(35,36,44) Peak broadening and new features in the second-order Raman spectrum of reduced size crystallites are observed and are also attributed to breakdown of the Raman selection rules.(41)

Amorphous Carbons. Amorphous carbon (a-C) materials exhibit a complete lack of the translational order associated with crystalline (even nanocrystalline) materials. However, due to the diversity of local (2-, 3-, and 4-coordination) bonding and the medium-range (. 5 Å to . 20 Å) ordering of carbon, a-C's exhibit a wide variety in their structures and properties.

Diamond-like carbon (d-C) films have wide technological applications which--like diamond--stem from their extreme properties including hardness, chemical inertness, smoothness and apparent impermeability.(4,7,23) While these properties of diamond-like films are often not as extreme as those of diamond films, the relative ease of fabrication and the ability to produce smooth, thin, uniform films often makes diamond-like films more attractive. Specific applications include use as anti-abrasion or anti-erosion coatings for computer disks and read-write heads, infrared windows and lenses, optical fibers and machine tools; low-friction coatings for prosthetics and bearing surfaces; cold cathode emitters; electrochemical electrodes; x-ray lithography; and thermal dissipation.

Graphitic amorphous carbon (g-C) is of fundamental interest as an elemental, 2D continuous random network (CRN) with only one type of atom and one dominant trigonal sp^2 bond type [see Fig. 1(c)] and as the prototype of a large class of covalently bonded CRN amorphous materials in which the disordered arrangement of atoms or molecules arises from highly directional covalent bonding stemming from low coordination number.(9,49) Two-dimensional CRN's have been most successfully applied to covalent inorganic glasses with binary compositions. g-C also has technical applications as a lubricant and as an inert electrode material. The structure of g-C is also of current technological interest because of its sibling relation to new forms of carbon solids (primarily, synthetic diamond and diamond-like films)

which are currently receiving intense development. Understanding g-C is essential, because it is a ubiquitous end product in most formation and processing of solid phases of carbon.

In general, evaporated and sputtered a-C prepared above 200 °C can be classified as g-C, whereas evaporated and sputtered a-C deposited at low temperatures and a-C prepared by CVD can be classified as sp^3-rich d-C (a few % to ~65%).(5,6,50) Hard amorphous carbon with higher concentrations of sp^3 bonding (to 85%) have been prepared using monoenergetic carbon beams and with plasma deposition (which contains hydrogen). This form of tetrahedral amorphous carbon is currently referred to as a-tC (51). Hydrogenated a-C (a-C:H),with H content of 20-50 atomic percent, is generally diamond-like with up to 70% sp^3 bonding. Hydrogen can be incorporated in substantial amounts during formation, usually from organic gas feed stock. When hydrogen content exceeds 50 atomic percent, films are polymer-like and exhibit strong broadband photoluminescence which can render collection of Raman spectra difficult. a-C evolves H at relatively low temperatures (150 EC to 400 EC) and exhibits transformation toward nanocrystalline graphite at modest annealing temperatures (500 EC to 750 EC).(42,52,53) Most hard a-C also becomes more graphitic in nature upon annealing.(42) Early annealing studies of d-C (42) and g-C (52,53) monitored changes in L_a using Raman spectroscopy.

Robertson provides a comprehensive review of the structure, characterization, and physical properties of a-C.(5,6,8,54) Extensive experimental efforts have yet to achieve a unified interpretation of the various structures of a-C (in particular, the relative amounts of sp, sp^2, and sp^3 bonding) and the theory is only in its infancy.(9)

The simplest structural form of amorphous carbon is g-G which is generally agreed to have almost exclusively sp^2 bonds. Several models of a-C incorporate graphitic islands or rafts formed from warped layers of 3-coordinated atoms arranged in quasi-2D CRN's with planar dimensions of 5 to 20 Å.(8,55-57) Bond lengths do not deviate appreciably from the graphite interplanar bond length (1.42 Å), however bond-angle distributions with 10E to 25E widths allow for the formation of significant numbers of 5- and 7-membered rings, and perhaps even some 4-, 8- or 9-membered rings. The presence of odd-membered rings and/or translational disorder suggests there should be small warping or bending within the rafts.(57) The different models suggest that the quasi-planar rafts are cemented together with varying concentrations of sp^3-bonded atoms (1% to 10% sp^3

bonding for g-C and up to 85% for d-C) which allow for changes in orientations of the raft planes without the necessity of dangling bonds or voids that would result from unconnected, randomly oriented planes; this results in mesoscopic isotropicity in g-C. The extent of layering within rafts or correlation of planes of adjacent rafts is not well known.

A recent examination of the large database of Raman fingerprinting experiments on hard amorphous carbon films by Tamor and Vassell (50) is a significant attempt at bringing order to our incomplete understanding of the structure of these materials. Their exhaustive treatment produces correlations between the Raman "G" and "D" bands and several important macroscopic quantities, notably the hardness and the bandgap. Analysis of these correlations support categorization of hard carbons as those possessing significant concentrations of hydrogen (a-C:H) and those which are not hydrogenated (d-C). They suggest these correlations allow Raman spectra to be used as a reliable predictor of hydrogenation, hardness, optical bandgap, and other properties.

The major features of the Raman spectra of various forms of a-C [see Figures 3(e) and 3(f)] appear to be related to similar features in the spectrum of graphite. They exhibit a broad, asymmetric peak centered near 1550 cm^{-1}. There are some differences in the Raman spectra of g-C, d-C and a-C:H including the breadth of the peak near 1550 cm^{-1} and the relative intensity of the low-frequency tail. a-C:H spectra exhibit a very broad feature centered roughly at 600 cm^{-1}. (50) Amorphous materials generally exhibit broad peaks, due to structural distributions and the breakdown of **k**=0 Raman selection rule.(9,40) The reduced Raman spectrum of amorphous materials often is a reasonable approximation of the single-phonon density of states. The broad spectra of a-C can be decomposed into two spectra centered near 1350 cm^{-1} and 1580 cm^{-1} which are often loosely associated with the graphite "G" and "D" peaks.(50) Such decompositions are not entirely justified and do not provide complete fits to the spectra. Doyle and Dennison have suggested an alternative decomposition based on the Raman active modes of planar, symmetric 5-, 6-, and 7-membered rings coupled to a surrounding network of carbon atoms; this work considers the structure of a-C in terms of ring statistics.(58)

Unfortunately, standard Raman spectroscopy does not as yet provide a sensitive method to determine the relative amounts of sp^2 and sp^3 bonding in a-C. The diamond sp^3 Raman cross

section is typically 50 to 100 times smaller than that of graphite sp^2 due to resonant Raman effects associated with the disparity in band gaps of the two materials (39); this precludes detection of small amounts of sp^3 bonding.(55) However, resonance Raman effects, as yet not well understood, are sensitive to the relative concentrations of sp^2- and sp^3-bonded carbon. Excitation in the infrared range results in high sensitivity to scattering from amorphous sp^2-bonded carbon whereas ultraviolet excitation enhances the diamond 1332 cm^{-1} peak considerably. (26,59,60) This effect has been discussed in terms of differing resonance effects for sp^2- and sp^3-bonded carbon or in relation to the size of clusters of sp^2-bonded carbon.

Fullerenes, Fullerites, Graphenes and Related Materials. The first order Raman spectrum of powdered C_{60} (61,62) [see Figure 3(g)] agrees well with group-theoretical analysis of the molecular spectrum (63-65). There are ten narrow first-order peaks observed which are assigned to the two nondegenerate A_g and eight fivefold degenerate H_g Raman active modes. Peak intensities are in good agreement with bond charge model calculations.(65) Peaks in the second order Raman spectra have been observed; many have been assigned.(63,64)

Fullerites are crystalline forms of carbon with fullerenes occupying each site in the unit cell. The first-order Raman spectrum of solid C_{60} is remarkable in that it is almost identical to that of the free molecule, providing strong evidence of the weak interactions between molecules within the solid. No significant changes are observed in the spectra by hydrostatic pressures up to 10 GPa, although small linear changes in peak positions with increasing pressure are observed (66). The first order phase transition at ~260 K, from a low temperature rotationally-ordered simple cubic (T^6_h) phase to a high temperature fcc (T^3_h) phase, where individual molecules are free to rotate, is marked by discontinuous changes in Raman peak positions and widths. (61,66) In addition, more than 100 weak Raman lines and a great deal of detailed structure are observed and have been variously assigned to second- and higher-order combination and overtone scattering from intramolecular vibrational modes, to broken-symmetry modes which are isotopically activated, to crystal-field induced splitting of the first-order Raman modes, or from the presence of merohedral disorder (61,67,68).

Raman spectroscopy has been used extensively in the characterization of other pure carbon structures. Related fullerene molecules (*e.g.*, C_{56}, C_{70}, C_{76}, C_{119}) and associated fullerite crystals

have spectra similar in nature to that of C_{60}, but are typically more complex due to lack of the extensive symmetries found in C_{60}. The same is true for the Raman spectra of nested fullerenes, molecules with two or more fullerenes inside one another.(14) Carbon nanotubules are cylindrical tubes--often nested--formed of rolled hexagonal sheets, often capped with C_{60}-like ends. The various forms of carbon nanotubules have Raman spectra similar to nanocrystalline graphite (15,69); this is not surprising, since almost all of the carbon atoms in nanotubules are in rolled graphite-like sheets.

SUMMARY

The utility of Raman spectroscopy for examining bulk structural and electronic properties of carbon (and other) solids has made great advances, undergoing a transition from a purely research field to an analytical diagnostic ("fingerprinting") tool. Much of the power of Raman measurements lies in its ability to simultaneously examine multiple structural phases coexisting within a given sample. Still, continued research is needed to better understand the exact nature of the various ubiquitous disordered forms of carbon solids which compete with, and often prevail over, crystalline phases. Instrumentation developments are forthcoming which will make Raman diagnosis more compact and suited to *in situ* applications in fabrication processes (70). Sub-Rayleigh resolution optical methods [*e.g.*, NSOM (30)] show promise for optically examining extremely small sample volumes.

ACKNOWLEDGMENTS

The authors wish to extend special thanks to T. Dallas (Texas Tech) for providing the spectra in Figure 3. Greg Swain acknowledges support from NSF (CHE-9505683), the Petroleum Research Fund (ACS-PRF 29493) and the DOD DURIP program (FY95). Mark Holtz also acknowledges support from the Petroleum Research Fund of the American Chemical Society. J.R. Dennison acknowledges partial support from the USU Faculty Research Council.

REFERENCES

(1) H.O. Pierson, *Handbook of Carbon, Graphite, Diamond and Fullerenes: Properties, Processing and Applications*, (Noyes Publications, Park Ridge, NJ, 1993).
(2) A.W. Moore, *Physics and Chemistry of Carbon*, (Dekker, New York, 1973).
(3) M.A. Short and P.L. Walker, Carbon **1,** 3 (1963).
(4) *Status and Applications of Diamond and Diamond-like Materials: An Emerging Technology*," National Materials Advisory Board NMAB-445 (National Academy Press, 1990).
(5) J. Robertson, Adv. Phys. **35**, 317 (1986).
(6) Th. Frauenheim *et al*., J. Non-Cryst. Solids, **182,** 186 (1995) .
(7) J.C. Angus and C.C. Hayman, Science **241,** 913 (1988).
(8) J. Robertson, Surf. Coatings Technol., **50,** 185 (1992).
(9) S.R. Elliott, *Physics of Amorphous Materials*, 2nd Ed. (Longman Scientific, London, 1990).
(10) S.R. Elliott, Nature **354,** 445 (1991).
(11) W. Kratschmer, L.D. Lamb, K. Fostiropoulos and D.R. Huffman, Nature (London) **347**, 354 (1990).
(12) H. Kroto *et al.* Nature (London) **318,** 162 (1988).
(13) H.W. Kroto and D.R.M. Walton, *The Fullerenes*, Cambridge University Press, Cambridge, 1993).
(14) W.A. de Heer and D. Ugarte, Chem. Phys. Lett. **207,** 480 (1993) .
(15) T.W. Ebbesen, Ann. Rev. Mat. Sci. **24**, 235 (1994).
(16) R.L. McCreery, in *Electroanalytical Chemistry*, A.J. Bard, Ed., Vol. 17 (Dekker, New York, 1991); R.L. McCreery and R.T. Packard, Anal. Chem. **61**, 775A (1989).
(17) H. Lock, *et al.* J.Chem. Phys. **99**, 3363 (1993); K.M. McNamara, *et al.* Diamond and Related Materials **1**, 1145 (1992).
(18) M. Cardona and G. Guentherodt in *Light Scattering in Solids II* (Springer, Berlin, 1982), p. 1).
(19) B. Chase, Appl. Spec. **48,** 14A (1994).
(20) S. Prawer, K.W. Nugent and P.S. Weiser, Appl. Phys. Lett **65**, 2248 (1994).
(21) M.Fryling, C.J. Frank and R.L. McCreery, Appl. Spec. **47**, 1965 (1993).
(22) B. Yang, M.D. Morris and H. Owen, Appl. Spectroscopy **45,** 1533 (1991)..
(23) R.F. Davis, *Diamond Films and Coatings*, Noyes Publications, Park Ridge, NJ, 1993).
(24) D.S. Knight and W.B. White, J. Mater. Sci. **4**, 385 (1989).
(25) S.A. Solin and A.K. Ramdas, Phys. Rev. B**1,** 1687 (1970).
(26) J. Wagner, C. Wild and P. Koidl, Appl. Phys. Lett., **59**, 779 (1991).
(27) M. Hanfland *et al.* Phys. Rev. B**31**, 6896 (1985).
(28) J.M. Botelerf and Y.M. Gupta, Phys. Rev. Lett. **71**, 3497 (1993).
(29) M.H. Grimsditch, E. Anastassakis, and M. Cardona, Phys. Rev. B **18**, 901 (1978).
(30) M. Yosikawa *et al.*, Appl. Phys. Lett. **55,** 2608 (1989).
(31) W.D. Duncan, J. Vac. Sci. Technol. ("*Amer. Vac. Soc. National Symp.*" Minneapolis, MN, Oct. 1995), in press.

(32) W.F. Banholzer and T.R. Anthony, Thin Solid Films **212**, 1 (1992).
(33) C.E. Johnson and W.A. Weimer, J. Electrochem. Soc. **141,** 2161 (1994).
(34) S.A. Solin in *"Graphite Intercalation Compounds I: Structure and Dynamics"*, Topics in Current Physics, edited by H. Zabel and S.A. Solin (Springer, Berlin, 1990), p. 157.
(35) R. Al-Jishi and G. Dresselhaus, Phys. Rev. B**26**, 4514 (1982) .
(36) R.J. Nemanich and S.A. Solin, Phys. Rev. B**20**, 392 (1979).
(37) M. Hanfland, H. Beister and K. Syassen, Phys. Rev. B**39,** 12598 (1989).
(38) R. Vidano and D.B. Fischbach, J. Am. Ceramic Soc. **61,** 13 (1978).
(39) K. Sinha and J. Menendez, Phys. Rev. B**41,** 10845 (1990).
(40) G.W. Jenkins and K. Kawamura, *Polymeric Carbons*, (Cambridge Un. Press, Cambridge, 1976).
(41) R.J. Nemanich, G. Lucousky and S.A. Solin, Mater. Sci. Eng. **31,** 157 (1977).
(42) R.O. Dillon, J.A. Woolam and V. Katkanant, Phys. Rev. B**29**, 625 (1984).
(43) D.S. Knight and W.B. White, J. Mater. Res. **4,** 4713 (1989).
(44) F. Tuinstra and J.L. Koenig, J. Chem. Phys. **53**, 1126 (1970).
(45) P. Lespade, R. Al-Jishi and M.S. Dresslehaus, Carbon, **20,** 427 (1982).
(46) R. Shuker and R.W. Gammon, Phys. Rev. Lett. **25**, 222 (1970).
(47) Yan Wang, D.C. Alsmeyer and R.L. McCreery, Chem Mater. **2**, 557 (1990).
(48) T. Dallas, M. Holtz, H. Ahn and M.C. Downer, Phys. Rev. B**49**, 796 (1994).
(49) R. Zallen, *The Physics of Amorphous Solids*, (Wiley, New York, 1983).
(50) M.A. Tamor and W.C. Vassell, J. Appl. Phys. **76**, 3823 (1994).
(51) D.R. McKenzie, D. Muller and B.A. Pailthorpe, Phys. Rev. Lett **67,** 773 (1991); M. Weiler, *et al.* Appl. Phys. Lett. **64,** 2797 (1994).
(52) J.N. Rouzard, A. Oberlin and C. Beny-Bassez, Thin Solid Films **105,** 75 (1983).
(53) N. Wada, J. Non-Cryst. Solids **53,** 543 (1980) .
(54) J. Robertson, Prog. Solid State Chem. **21,** 199 (1991).
(55) D. Beeman, J. Silverman, R. Lynds and M.R. Anderson, Phys. Rev. B**30,** 870 (1984).
(56) J. Tersoff, Phys. Rev. Lett. **61,** 2879 (1988).
(57) G. Galli, R.M. Martin, R. Car and M. Pairnelto, Phys. Rev. Lett. **62,** 555 (1989).
(58) T.E. Doyle and J.R. Dennison, Phys. Rev. B**51**, 196 (1995).
(59) M. Tamor, J.A. Haire, C.H.Wu and K.C. Hass, Appl. Phys. Lett., **54**, 12 (1989).
(60) J. Wagner, M. Ramsteiner, C. Wild and P. Koidl, Phys. Rev. B**40,** 1817 (1989).
(61) Z.-H. Dong *et al.* Phys. Rev. B**48**, 2862 (1993).
(62) W.S. Bacsa, W.A. de Heer, D. Ugarte and A. Chatelain, Chem. Phys. Lett. **211**, 346 (1993).
(63) G. Dresselhaus, M. Dresselhaus and P.C. Eklund, Phys. Rev. B**45,** 6923 (1992).
(64) P.C. Eklund *et al.* Molecular Crystals and Liquid Crystals Science and Technology, Section A-Molecular Crystals and Liquid Crystals, **25,** 199 (1994).
(65) S. Sanguinett, G. Benedekl and E.Finnagall, J. Elec. Spect. Rel. Phenom. **64/65** (1993) 899; Phys. Rev. B**50,** 6743 (1994).
(66) S.H. Tolbert *et al.* Chem. Phys. Lett. **188,** 163 (1992).
(67) P.H.M. van Loosdrecht *et al.* Chem. Phys. Lett. **198,** 587 (1992).
(68) P.J. Horoyski, L.W. Thewalt and T.R. Anthony, Phys. Rev. Lett. **74,** 194 (1995).
(69) H. Hiura, T.W. Ebbesen, K. Tanigaki and H. Takahashi, Chem. Phys. Lett. **202,** 509

(1993).
(70) J.R. Ferraro, Spectroscopy **11**(3), 18 (1996).

J.R. Dennison *is an associate professor of physics at Utah State University. He received his Ph.D. in 1985 from Virginia Tech. His research interests include the structure and dynamics of disordered and amorphous materials and physisorbed layers and electron scattering.*
Mark Holtz *is an assistant professor of physics at Texas Tech University. He received his Ph.D. from Virginia Tech in 1987. He conducts research using Raman and photoluminescence spectroscopies to study the effects of disorder and pressure on carbon and semiconducting solids.*
Greg Swain *is an assistant professor of analytical chemistry at Utah State University. He received his degree from the University of Kansas in 1991. His research has focused on the electrochemical properties of carbon electrodes, in particular diamond and diamond-like carbon thin films.*

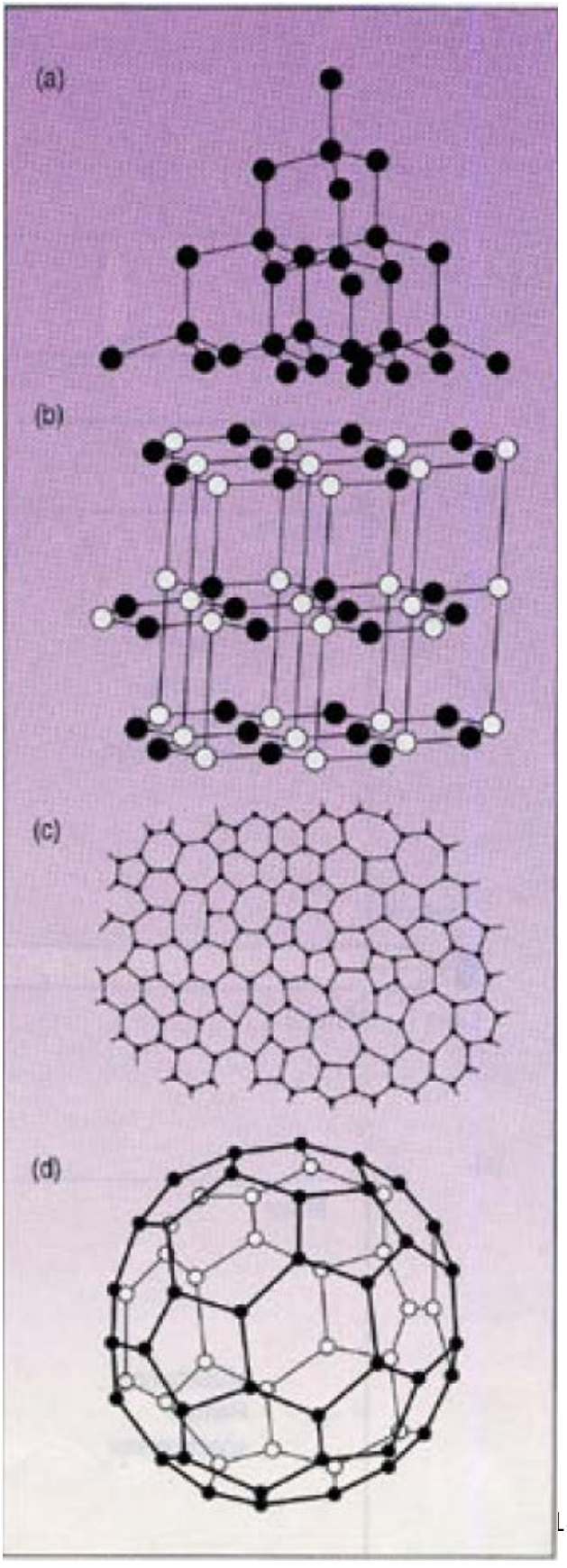

Figure 1. Structures of solid carbon: **(a)** fcc diamond lattice, **(b)** hexagonal graphite lattice, **(c)** 2D continuous random network structure of graphitic amorphous carbon, **(d)** truncated icosahedron structure of C_{60} molecule.

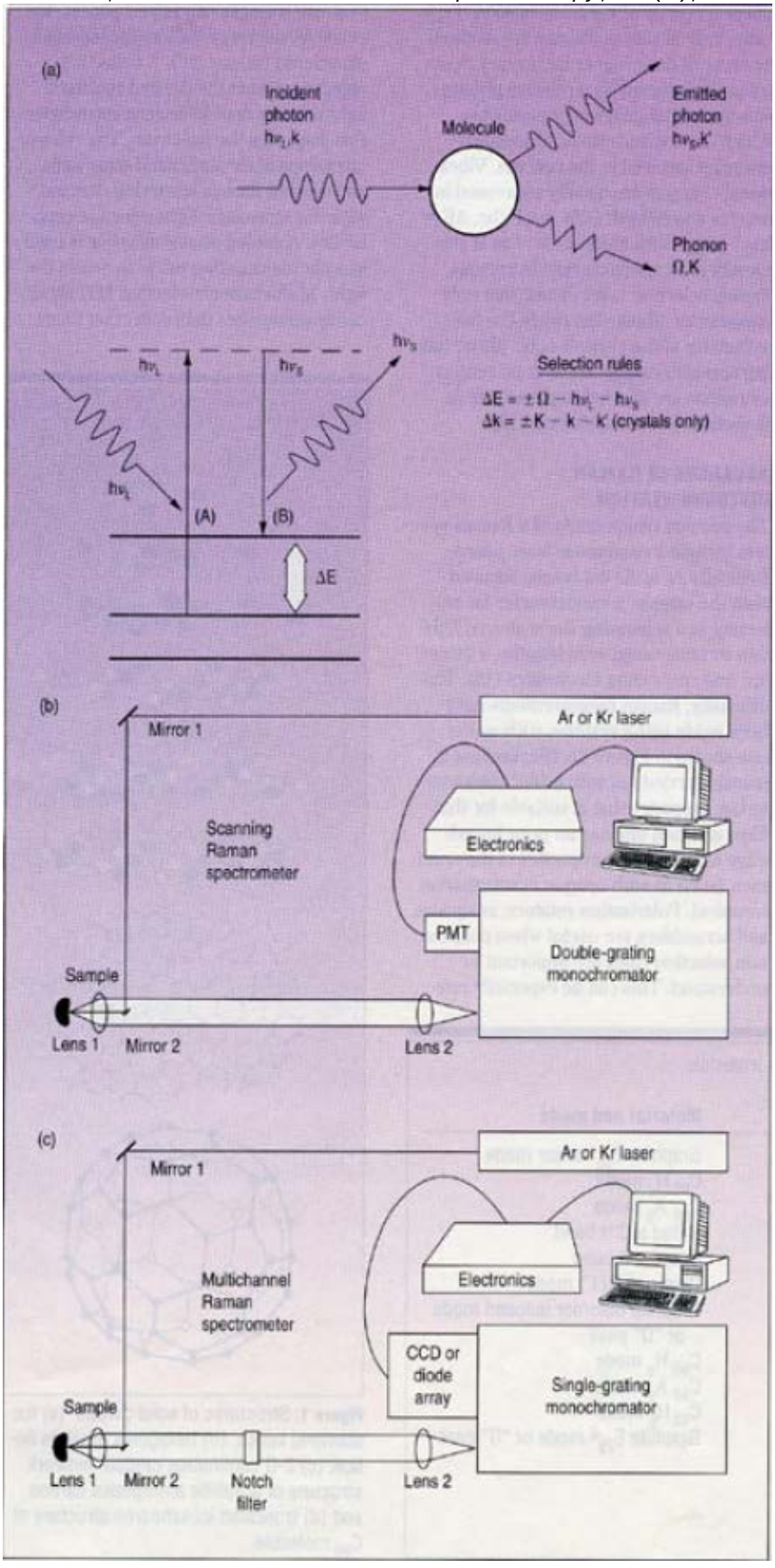
(a)
Incident photon
Molecule
Emitted photon
Phonon
Selection rules
(A)
(B)
ΔE
(b)
Mirror 1
Ar or Kr laser
Scanning Raman spectrometer
Electronics
PMT
Double-grating monochromator
Sample
Lens 1
Mirror 2
Lens 2
(c)
Mirror 1
Ar or Kr laser
Multichannel Raman spectrometer
Electronics
CCD or diode array
Single-grating monochromator
Sample
Lens 1
Mirror 2
Notch filter
Lens 2

Figure 2. Raman spectroscopy: **(a)** Stokes and anti-Stokes energy level diagrams of the Raman process. Schematic diagrams of Raman instrumentation with **(b)** double-stage monochromator and **(c)** single-stage grating monochromator.

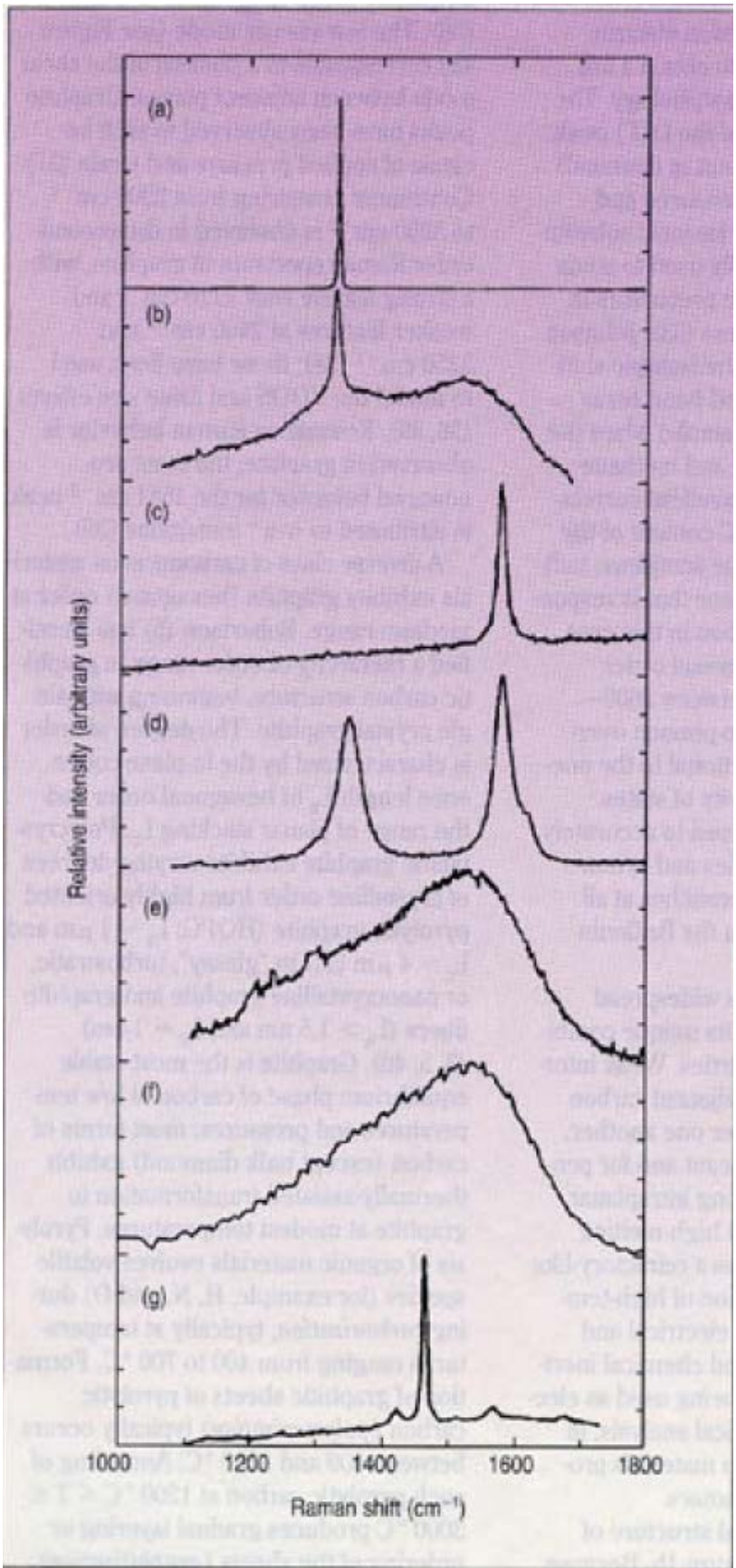

Figure 3. First order Raman spectra of solid carbon using the 2.41 eV Ar ion laser excitation: **(a)** diamond, **(b)** CVD microcrystalline diamond film, **(c)** single crystal graphite, **(d)** nanocrystalline graphite with in-plane coherence length of 20 nm, **(e)** arc evaporated graphitic amorphous carbon, **(f)** ion sputtered diamond-like amorphous carbon, **(g)** powdered C_{60}.

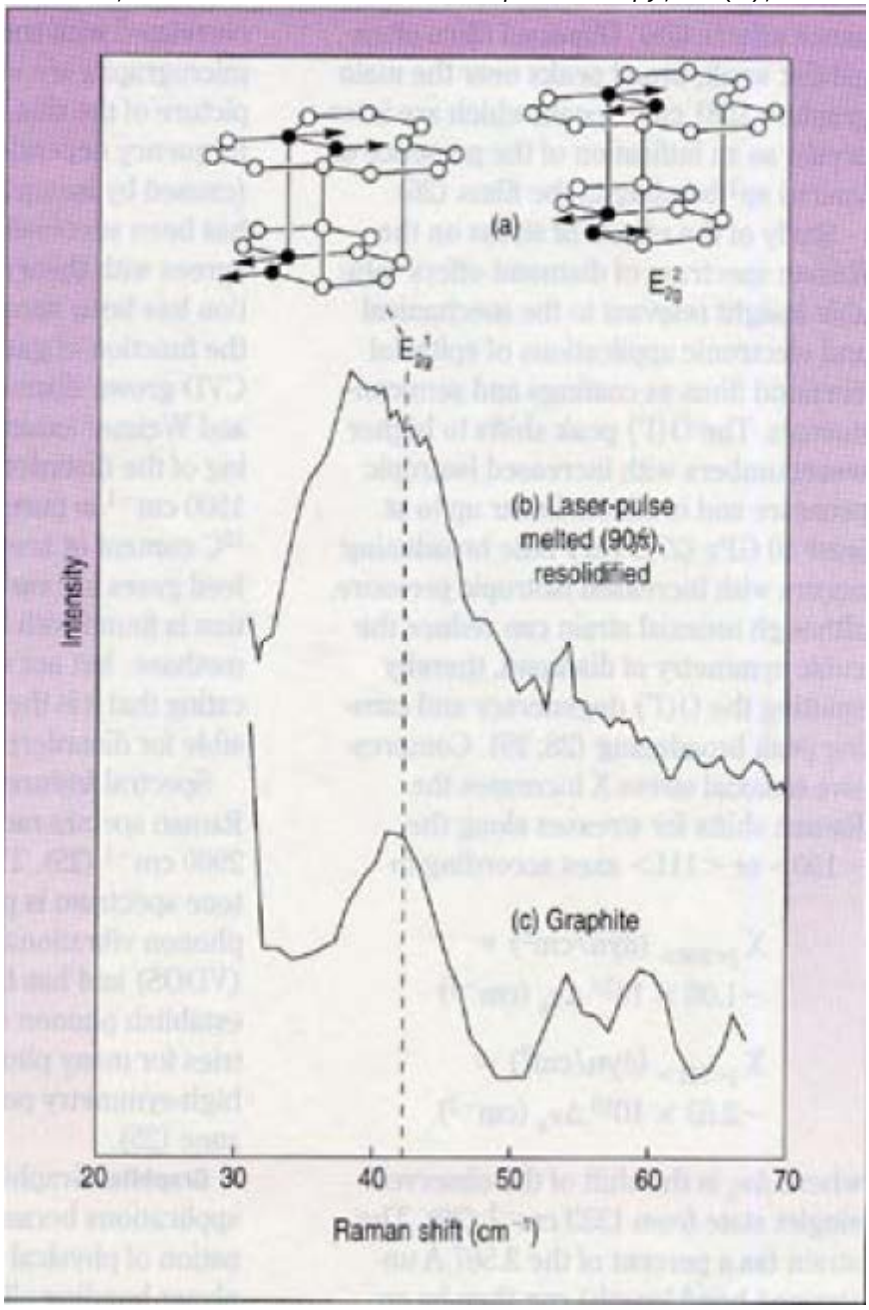

Figure 4. **(a)** Raman active vibrational E^1_{2g} and E^2_{2g} modes of graphite. Raman spectra of the graphite E^1_{2g} shear mode for **(b)** nanocrystalline graphite with in-plane coherence length L_a . 6.0 nm and out-of-plane coherence length L_c . 0.85 nm and **(c)** graphite. Adapted from Reference 48.

Table 1: Characteristic Raman Features of Carbon Materials

Wavenumber (cm^{-1})	Strength [a]	Material and Mode
42	vw	Graphite E_{2g}^1 shear mode
272	w	C_{60} H_g mode
496	w	C_{60} A_g mode
~600	w	Broad a-C:H band
~1200 to 1600	s	Broad a-C band
1333	s	Diamond O(Γ) mode
~1360[b]	vs	Graphite disorder induced mode or "D" peak
1424	w	C_{60} H_g mode
1468	vs	C_{60} A_g mode
1574	w	C_{60} H_g mode
1581	vs	Graphite E_{2g}^2 mode or "G" peak

[a] vs-very strong, s-strong, w-weak, vw-very weak [b] Dependant on excitation wavelength